



Cite this: *Catal. Sci. Technol.*, 2018, 8, 4812



## Carbon-based SILP catalysis for the selective hydrogenation of aldehydes using a well-defined Fe(II) PNP complex

Rafael Castro-Amoedo,<sup>†,a</sup> Zita Csendes,<sup>†,a</sup> Julian Brünig,<sup>a</sup> Markus Sauer,<sup>ID, b</sup> Annette Foelske-Schmitz,<sup>b</sup> Nevzat Yigit,<sup>c</sup> Günther Rupprechter,<sup>c</sup> Tushar Gupta,<sup>c</sup> Ana Margarida Martins,<sup>ID, d</sup> Katharina Bica,<sup>ID, a</sup> Helmuth Hoffmann<sup>\*a</sup> and Karl Kirchner<sup>ID, \*a</sup>

In this work, the supported ionic liquid phase (SILP) method was applied for the immobilization of a newly developed, well-defined hydride Fe(II) PNP pincer complex dissolved in ionic liquid (IL) onto polymer-based spherical activated carbon. This novel SILP catalyst was structurally characterized by electron microscopy, N<sub>2</sub> adsorption-desorption, FTIR, and XPS measurements and was used for the hydrogenation of aldehydes to alcohols. For an optimized pore filling degree, this system showed excellent activity in the chemoselective hydrogenation of different aldehydes and proved to be reusable in at least seven consecutive reaction cycles without any loss in activity. Significantly lower reaction rates were observed, however, compared to a recent study of the same catalyst supported on silica, which was ascribed to the different pore sizes of these two support materials.

Received 23rd April 2018,  
Accepted 26th August 2018

DOI: 10.1039/c8cy00818c

[rsc.li/catalysis](http://rsc.li/catalysis)

### Introduction

The catalytic reduction of carbonyl groups using molecular hydrogen represents a way to obtain valuable alcohols, used for the production of bulk and fine chemicals in a green and economical way.<sup>1</sup> This reaction is typically catalyzed by both precious metal<sup>2</sup> and earth-abundant non-precious metal catalysts.<sup>3,4</sup> Our group recently reported the application of [Fe(PNP<sup>Me</sup>-iPr)(CO)(H)(Br)] (1) and *trans*-[Fe(PNP<sup>Me</sup>-iPr)(H)<sub>2</sub>-(CO)] (2) as (pre-)catalysts for the homogeneous, chemoselective hydrogenation of aldehydes.<sup>5</sup> The dihydride complex 2 is rapidly formed from 1 in the presence of H<sub>2</sub> and DBU (1,8-diaza-bicyclo[5.4.0]undec-7-ene) as base and is the actual catalyst. These complexes were found to be among the most efficient catalysts published to date. Nevertheless, the major drawback of homogeneous catalysts is the need for their separation at the end of the catalytic process. This shortcoming can be eliminated by immobilizing transition metal

complexes onto different supports.<sup>6</sup> However, the activity of a sensitive homogeneous catalyst is often decreased or lost upon its direct immobilization, since the active compound suffers a modification of its chemical and physical properties.

Ionic liquids (ILs) have attracted much attention as alternative efficient and benign reaction media for the immobilization of homogeneous catalysts for various catalytic reactions, either in liquid-liquid biphasic processes or for the design of supported liquid catalysts.<sup>7</sup> In the supported ionic liquid phase (SILP) technology, the homogeneous catalyst is dissolved in the ionic liquid and deposited on a mesoporous solid material; thus, its chemical nature can be preserved, while the applied solvent is not miscible with the IL and is enriched with the product of the catalyzed reaction. SILP catalysis allows for a straightforward separation of the product from the transition metal complex; moreover, the high surface area provided by the mesoporous support material results in high reactivity. In general, it may be considered as green and sustainable technology, since it combines the main advantages of heterogeneous and homogeneous catalysis, providing a homogeneous environment for the reaction that is particularly well suited for gas phase continuous flow processes with fixed-bed reactor set-up.<sup>8</sup>

A number of different support materials can, and have been, used for the preparation of SILP catalysts, including silica, carbon, alumina or titanium based porous materials as well as their combinations. While amorphous silica-based materials are by far the most popular choice, the acidic

<sup>a</sup> Institute of Applied Synthetic Chemistry, Vienna University of Technology, Getreidemarkt 9, A-1060 Vienna, Austria.

E-mail: [helmut.hoffmann@tuwien.ac.at](mailto:helmut.hoffmann@tuwien.ac.at), [karl.kirchner@tuwien.ac.at](mailto:karl.kirchner@tuwien.ac.at)

<sup>b</sup> Analytical Instrumentation Center, Vienna University of Technology, Getreidemarkt 9, A-1060 Vienna, Austria

<sup>c</sup> Institute of Materials Chemistry, Vienna University of Technology, Getreidemarkt 9, A-1060 Vienna, Austria

<sup>d</sup> Centro de Química Estrutural, Instituto Superior Técnico, Universidade de Lisboa, Av. Rovisco Pais No. 1, 1049-001 Lisboa, Portugal

† These authors contributed equally.

surface composition might interfere with the catalytic reaction or with the catalyst itself, particularly when sensitive species such as well-defined base metal catalysts are involved. Activated carbon materials are promising supports for SILP catalysis because of their high surface area, stability, inertness, and adsorption capacity.<sup>9</sup> These can be easily customized for the particular reaction since their surface area, pore volume and surface chemistry are tunable. The leaching of both IL and catalyst can be negligible by applying carbon supports with high volumes of supermicro and mesopores.<sup>10</sup> Most recently, Weiß *et al.* showed that undesired side reaction in the gas phase hydroformylation of ethylene could be avoided by replacing silica-based SILP catalysts with nitrogen-doped carbon materials and emphasized the importance of support chemistry for long-term stability in industrially viable processes.<sup>11</sup>

In this work, we present the preparation, characterization, and application of complex **1** immobilized in an activated carbon SILP system. To the best of our knowledge, this is the first example of a well-defined Fe(II) complex applied as a carbon-based SILP system for the selective hydrogenation of aldehydes to afford alcohols.

## Experimental

### Materials

All manipulations were performed under argon atmosphere using Schlenk techniques or/and in a MBraun inert-gas glovebox. All solvents were purified according to standard procedures.<sup>12</sup> The deuterated solvents were purchased from Aldrich and dried over 4 Å molecular sieves. The IL, 1-ethyl-2,3-dimethylimidazolium bis(trifluoromethylsulfonyl)imide ( $[C_2m_2im][NTf_2]$ ), 99% purity, was purchased from IoLiTec and was dried for at least 24 h at room temperature and  $\sim 10^{-2}$  mbar before use and was stored under an argon atmosphere. Polymer-based spherical activated carbon (CARB) was used as support (donated by Blücher GmbH) and was degassed under vacuum at 300 °C for 6 h. The complex  $[Fe(PNP^Me-iPr)(CO)(H)(Br)]$  (**1**) was prepared according to the literature.<sup>5</sup> All aldehyde substrates were obtained from commercial sources and purified by distillation prior to use. Hydrogen (99.999% purity) was purchased from Messer Austria and used as received.

### Catalyst preparation

In order to find the optimum impregnation of the support, 5 mg complex **1** and 30–60  $\mu$ l IL in 2 ml ethanol were added to 100 mg CARB and stirred for 5 minutes, under inert atmosphere. Then, the solvent was evaporated under vacuum ( $\sim 10^{-2}$  mbar) at 60 °C until the spheres presented rolling behavior again ( $\sim 10$  min).

### Material characterization

Scanning electron microscopy (SEM) images were acquired using FEI Quanta 250 FEGSEM scanning electron microscope

at 5 kV. Transmission electron microscopy (TEM) images were obtained using FEI TECNAI F20 transmission electron microscope at 200 kV. The sample was mildly grinded to preserve the porous structure and stirred in ethanol for 6 hours then sonicated for 30 minutes to ensure an optimal dispersion. Two drops from the well dispersed top part were taken and dropped in a copper Lacey carbon-coated grid. X-ray photoelectron spectroscopy (XPS) measurements were carried out on a SPECS XPS-spectrometer equipped with a monochromatized Al-K $\alpha$  X-ray source ( $\mu$ Focus 350) and a hemispherical WAL-150 analyzer (acceptance angle: 60°). Samples were mounted onto the sample holder using double-sided Cu tape or Ta. Pass energies of 100 eV and 30 eV and energy resolutions of 1 eV and 100 meV were used for survey and detail spectra respectively (excitation energy: 1486.6 eV, beam energy and spot size: 70 W onto 400  $\mu$ m, angle: 51° to sample surface normal, base pressure:  $6 \times 10^{-10}$  mbar, pressure during measurements:  $2 \times 10^{-9}$  mbar). Data analysis was performed using CASA XPS software packages employing Shirley backgrounds<sup>13</sup> and Scofield sensitivity factors.<sup>14</sup> Charge correction was applied, so the adventitious carbon peak (C–C peak) was shifted to 284.8 binding energy (BE). Curve fits using combined Gaussian–Lorentzian peak shapes were used to discern the components of detail spectra. To reduce charging effects a broad spot low energy electron source (SPECS FG 22 flood gun) was used for charge compensation (5 eV/25  $\mu$ A). The detection limit in survey measurements lies around 0.1–0.5 at%, depending on the element. The accuracy of XPS measurements is around 10–20% of the values shown, and the maximum depth is about 7–10 nm.

$^1H$ ,  $^{19}F\{^1H\}$ , and  $^{31}P\{^1H\}$  NMR spectra were recorded on Bruker AVANCE-250 spectrometer.  $^1H$  spectra were referenced internally to residual protic-solvent resonances and are reported relative to tetramethylsilane ( $\delta = 0$  ppm).  $^{31}P\{^1H\}$  NMR spectra were referenced externally to  $H_3PO_4$  (85%) ( $\delta = 0$ ).  $^{19}F\{^1H\}$  spectra were referenced externally to trifluorotoluene (0.05%) ( $\delta = 0$  ppm).

FTIR spectra were recorded in diffuse reflectance with a Bruker Vertex 80 FTIR spectrometer using a narrow band MCT detector and a Harrick Seagull reflection optical unit. The scanned wavenumber range was 4000  $cm^{-1}$  to 800  $cm^{-1}$ . 256 scans were collected for each spectrum with 4  $cm^{-1}$  resolution. The spectra were baseline corrected.  $N_2$  adsorption–desorption isotherms were measured at 77 K with a volumetric adsorption analyzer (Micromeritics, ASAP 2020) using the Brunauer–Emmett–Teller (BET) theory for determining the surface area and the non-local density functional theory (NLDFT) method for calculating the pore size distribution and pore volumes. Fe leaching was monitored using an inductively coupled plasma (ICP) optical emission spectrometer PerkinElmer OPTIMA 8300 equipped with an SC-2 DX FAST sample preparation system. A customized single-element (Merck, Roth) standard was used for the calibration. All samples were extracted using ethanol and methanol (two times each), followed by solvent-evaporation and acid-digestion ( $HNO_3$  and  $H_2O_2$  at a 2:1 ratio).

## General procedure for the hydrogenation of aldehydes

All hydrogenation reactions were performed in a Carl Roth 100 ml autoclave at room temperature (25 °C), under hydrogen pressures between 10 to 40 bar. For preparing the reaction mixture, a vial was charged with the impregnated support or catalyst dissolved in IL and was placed in the autoclave. Then, the autoclave was evacuated and flushed with argon three times. Subsequently, 5 mol% DBU, 2 ml heptane and 2 mmol aldehyde were taken up into a syringe and injected into the autoclave. After flushing it three times with hydrogen, the desired hydrogen pressure was established, and the reaction was carried out for the stated time. Afterward, the hydrogen gas was released, and the sample was analyzed by  $^1\text{H}$  and/or  $^{19}\text{F}\{^1\text{H}\}$  NMR spectroscopy to determine the conversions by integrating the aldehyde and alcohol signals.

## Results and discussion

### Characterization of the support

Fig. 1 shows electron microscopy images of the untreated CARB support employed in this study. It consists of evenly-sized carbon spheres with diameters of about 400  $\mu\text{m}$ . In the TEM image (Fig. 1B), the microcrystalline nature is clearly evident from the superimposed grid pattern corresponding to the graphitic carbon layers. On top of that, a larger-sized pattern of parallel light and dark stripes with a distance of about 1 nm can be seen, in particular at the outer edges of the particle in Fig. 1B, which indicates the presence of micropores. However, it must be emphasized here that the native porous structure of the carbon spheres is probably at least partly destroyed in the process of TEM sample preparation.

An important task in this work was to determine the surface composition of CARB, since, depending on their nature, surface groups can interact with the catalyst, IL, substrate, and product. Complex 1 is very sensitive to highly coordinating and/or acidic groups such as carboxyl and phenol groups. XPS measurements were used to determine the atomic composition of the surface and to quantify the carbon bonds on the surface. It was found that the surface (to a depth of 7–10 nm) of CARB contains 94 at% C, 5 at% O, and <1 at% other elements. Analysis of the C 1s detail spectrum of CARB (Fig. 2) revealed that the carbon signal mostly consists of

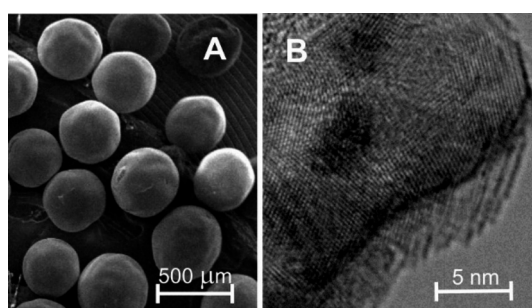


Fig. 1 SEM image (A) and TEM image (B) of CARB, a polymer-based spherical activated carbon.

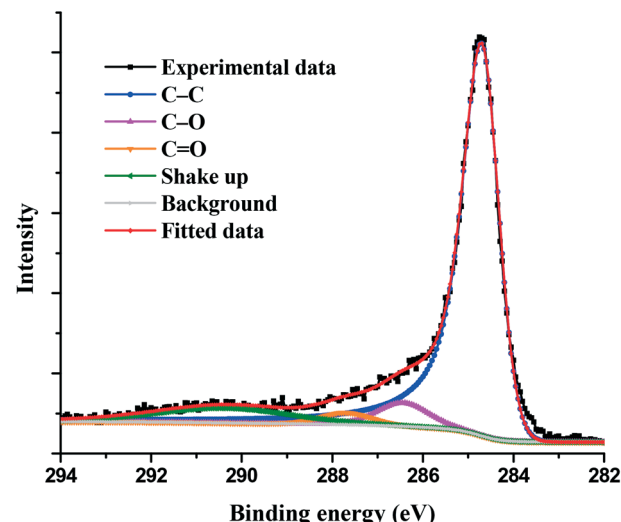


Fig. 2 C 1s spectrum of CARB.

three major components corresponding to three different bonding environments: C-C at 284.7 eV (78 at%), C-O at 286.4 eV (7 at%), and C=O at 287.7 eV (4 at%).<sup>15</sup> In addition, we could evidence a shakeup peak around 290.4 eV (11.5 at%).

The lack of an O-C=O peak at ~289 eV suggests that the surface does not contain strongly acidic functionalities such as carboxylic, anhydride, lactone and lactol groups, which in turn are extremely dangerous to our catalyst. This absence is in good agreement with the 900 °C heat treatment used in the activation step of the carbon spheres since this high temperature can selectively remove these acidic groups from the activated carbon surface.<sup>16</sup> However, some weakly acidic phenol groups may be present on the surface, since the carbon signal contains 7 at% C-O bonds which can be attributed to phenol and ether functionalities. The C=O bonds are likely due to ketones and quinones. The pH value of CARB was found to be 8.4 which confirms the overall presence of more basic than acidic groups making the support suitable for our catalytic applications without further modification.<sup>17</sup>

The shape of the  $\text{N}_2$  adsorption–desorption isotherm of CARB (Fig. 3A) is of type I + IV according to the IUPAC classification, which is characteristic of materials with micro- and mesoporosity.<sup>18</sup> Due to the presence of micropores, larger adsorption occurs at low adsorbate pressures, while at higher pressures capillary condensation takes place in the mesopores. The steep increase of the isotherm close to the saturation pressure represents the pore filling of large meso/small macropores with pore diameters of 50 nm and above. The BET surface area and the available micro/mesopore volumes of the material were calculated from the isotherm and are listed in Table 1.

We can conclude so far that CARB is a promising candidate for SILP catalysis. It lacks acidic surface groups and does not require functionalization under harsh conditions. Moreover, it has a large surface area and contains a high amount of micropores, which offers stability against IL leaching.<sup>10</sup>



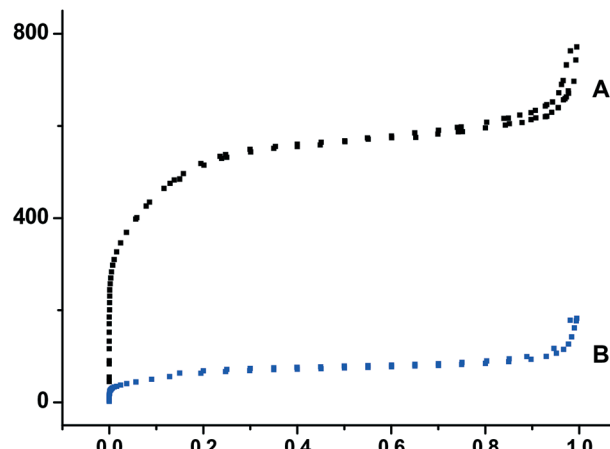


Fig. 3  $\text{N}_2$  adsorption–desorption isotherm of CARB (A) and CARB80 (B).

### Optimizing the impregnation of CARB

The second task was to find the optimum impregnation conditions regarding the amount of ionic liquid and the resulting pore filling degree of the carbon support. The hydrogenation of 4-fluorobenzaldehyde with complex **1** as pre-catalyst at 10 bar hydrogen pressure and 3 h reaction time was chosen to compare SILP catalysts with different IL loadings (Table 2). In light of the common sensitivity of aldehydes towards highly basic conditions, DBU (1,8-diazabicyclo[5.4.0]undec-7-ene) was found to be a suitable co-catalyst (base).<sup>5</sup> In fact, it has to be noted that the hydrogenation of cinnamaldehyde did not proceed in the presence of *t*BuOK, revealing the benefits of employing DBU as base in all reactions as reported previously.<sup>5</sup> As solvent *n*-heptane was used since neither the catalysts nor the IL were soluble in this solvent and leaching was not observed (*vide infra*), whereas both substrates and products were highly soluble in this solvent.

In entries 1–4, the amount of IL ( $V_{\text{IL}}$ ) was changed, keeping the amount of support and catalyst constant ( $m_{\text{CARB}} = 100$  mg,  $m_{\text{CAT}} = 5$  mg) in order to find the optimum IL loading. It is clearly seen that full conversion was achieved in 3 h when CARB was impregnated with 80 weight percent IL/cat 1 solution. We refer to this material as CARB80. At both lower and higher IL loadings, the conversion drops rapidly, similar to a recent study of our group using silica as support material.<sup>21</sup> The sharp maximum of conversion as a function of IL loading observed here is believed to be directly related to the pore structure and pore size distribution of the carbon support and can be qualitatively understood as follows: at low IL load-

ings, the IL/catalyst solution is contained mostly in micropores, which are filled from bottom to top and have only a small interface area with the surrounding reactant solution and yield accordingly low reaction rates. Once the micropores are completely filled, the mesopores get filled by adsorption of the IL/catalyst solution at the inner pore walls. This is where the catalyst has its highest activity due to the comparatively large interface area with the reactant solution. At even larger IL loadings, also the meso- and macropores get completely filled and the catalyst activity drops again.

### Characterization of CARB80

Structural parameters derived from the  $\text{N}_2$  adsorption–desorption isotherm (Fig. 3B, Table 1) showed that both the BET surface area and the total pore volume decreased after IL/catalyst impregnation due to the coating of the carbon surface and the clogging of micropores. The presence of blocked pores means that there are pores inside CARB80 which do not contain IL but are not accessible to  $\text{N}_2$ . This behavior is likely for microporous materials with pore diameters smaller than the size of the IL molecules. It also explains the discrepancy between the experimental pore filling degree of 76% (Table 1) compared to the nominal value of 42% (Table 2) for CARB80.

FTIR measurements (Fig. 4) clearly support a successful impregnation of the IL/catalyst inside the porous carbon substrate, since characteristic peaks of  $[\text{C}_2\text{m}_2\text{im}][\text{NTf}_2]$  (Fig. 4A) can be seen in the spectrum of CARB80 (Fig. 4B). The strong peaks between 1400 and 1000  $\text{cm}^{-1}$  are related to the vibrations of the  $[\text{NTf}_2]$  anion.<sup>19</sup> The peak at 1054  $\text{cm}^{-1}$  is assigned to the asymmetric stretch of the SNS group, the vibration at 1190  $\text{cm}^{-1}$  corresponds to the asymmetric  $\text{CF}_3$  stretch while the bands at 1350 and 1140  $\text{cm}^{-1}$  belong to the asymmetrical and symmetrical  $\text{SO}_2$  stretching vibration, respectively. The peaks between 1600 and 1400  $\text{cm}^{-1}$  are related to the cation  $[\text{C}_2\text{m}_2\text{im}]$  and include the highly characteristic CC/CN coupled stretching mode of the imidazolium ring at 1587  $\text{cm}^{-1}$  and the  $\text{CH}_2$  scissors deformation  $\delta(\text{CH}_2)$  at 1470  $\text{cm}^{-1}.$ <sup>20</sup> However, the peaks of complex **1** are essentially invisible in the spectrum of CARB80 due to its low concentration in the impregnated SILP material.

XPS measurements were used to analyze the surface composition of CARB80. CARB80 shows decreased C content and increased O content compared to the unaltered CARB. The sample also exhibits 6.3 at% F, 2.7 at% N and 1.4 at% S, indicating that a significant amount of IL is present in the porous carbon. It was found that the N 1s detail spectrum of

Table 1 Structural parameters calculated from the  $\text{N}_2$  adsorption–desorption isotherms

Sample	$S_{\text{BET}}^a$ ( $\text{m}^2 \text{ g}^{-1}$ )	$V_{\text{total}}^b$ ( $\text{cm}^3 \text{ g}^{-1}$ )	$V_{\text{nmp}}^c$ ( $\text{cm}^3 \text{ g}^{-1}$ )	$V_{\text{sup}}^d$ ( $\text{cm}^3 \text{ g}^{-1}$ )	$V_{\text{meso}}^e$ ( $\text{cm}^3 \text{ g}^{-1}$ )	$\alpha_{\text{exp}}^f$ (%)
CARB	1728	1.18	0.10	0.55	0.33	0
CARB-80	218	0.28	0.01	0.06	0.13	76

<sup>a</sup> BET surface area. <sup>b</sup> Total pore volume,  $\text{N}_2$  volume adsorbed at  $p/p^0 = 0.98$ . <sup>c</sup> Narrow micropore ( $<0.7 \text{ nm}$ ) volume. <sup>d</sup> Supermicropore ( $0.7 < d < 2 \text{ nm}$ ) volume. <sup>e</sup> Mesopore ( $2 < d < 50 \text{ nm}$ ) volume. <sup>f</sup> Experimental pore filling degree =  $[V_{\text{total}}(\text{CARB}) - V_{\text{total}}(\text{CARB80})]/V_{\text{total}}(\text{CARB}) \times 100$ .



Table 2 Influence of the IL loading in the SILP hydrogenation of 4-fluorobenzaldehyde

Entry	$V_{IL}$ (μl)	$\varepsilon^a$	$\alpha^b$ (%)	Time (min)	Conversion (%)	2 mmol
						<chem>CC1(C)N(C(C)(C)P(=O)(O)C)C2=C1C=CC=C2Br</chem>
1	30	50	25	180	6	
2	40	65	34	180	8	
3	50	80	42	180	>99	
4	60	95	51	180	22 <sup>c</sup>	

<sup>a</sup> IL loading =  $[(m_{IL} + m_{cat})/m_{CARB}] \times 100$ . <sup>b</sup> Pore filling degree =  $[V_{IL}/(V_{total} \times m_{CARB})] \times 100$ . <sup>c</sup> IL leaching observed by ICP-OES.

CARB80 contained two components at 399.0 eV and 401.4 eV corresponding to  $[NTf_2]$  and  $[C_2m_2im]$ , respectively (Fig. 5A). The F 1s detail spectrum (Fig. 5B) shows one component at 689.0 eV which is attributed to the  $[NTf_2]$  anion. The catalyst complex **1** in the CARB80 sample, however, is below the detection limit of XPS.

### Hydrogenations using CARB80 as catalyst

As previously described,<sup>5</sup> the first step of the catalytic cycle is the activation of catalyst **1** to form the *trans*-dihydride complex **2** which is the catalytically active species. The performance of this catalyst in the carbon-based SILP matrix (CARB80) was tested in the room temperature hydrogenation of different aromatic aldehydes to the corresponding alcohols in *n*-heptane solution and was compared to the results of a previous study of the same catalyst in a silica-based SILP matrix.<sup>21</sup> These results are presented in Table 3.

Aldehyde **A1** (4-fluorobenzaldehyde) was used to investigate the influence of the hydrogen pressure and the substrate/catalyst (*S/C*) ratio (entries 1–5). Doubling the pressure from 10 to 20 bar boosts up the conversion by a factor of 5, whereas a further pressure increase to 30 and 40 bar has a comparatively small effect. Increasing the *S/C* ratio from 200 to 1000 at 40 bar hydrogen pressure yields only a moderate increase in the TON and TOF values and a substantial drop of the reaction yield (entry 5). Quantitative conversion with 10 bar  $H_2$  pressure and *S/C* = 200 is reached for a reaction time of 3 h (entry 6). In a previous study,<sup>21</sup> this reaction was carried out under comparable conditions with silica instead of carbon as the support material and an approximately 10-fold faster conversion was observed (entry 7). Finally, we have also compared the hydrogenation of some other aromatic aldehydes **A2–A4** under identical reaction conditions for carbon and silica supports (entries 8–13). If present, C=C double bonds remained unaffected, as in the case of the challenging  $\alpha,\beta$ -unsaturated cinnamaldehyde (**A4**). Ketones, nitriles, esters and amides were not hydrogenated under these reaction conditions as already

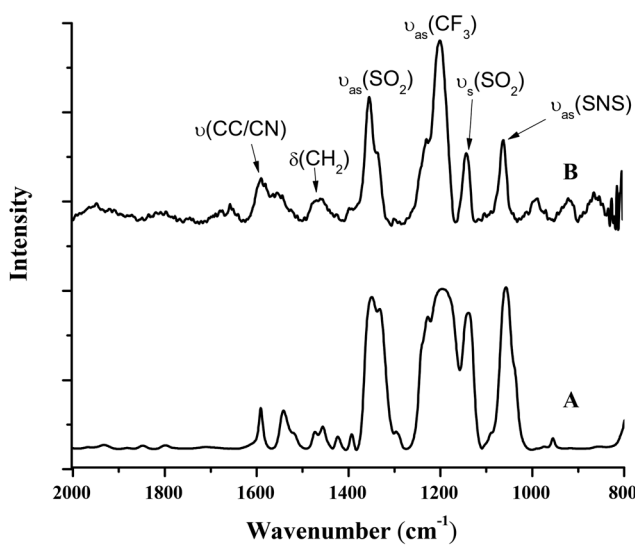


Fig. 4 FTIR spectra of A)  $[C_2m_2im][NTf_2]$  and B) CARB80 (the spectrum of CARB was subtracted).

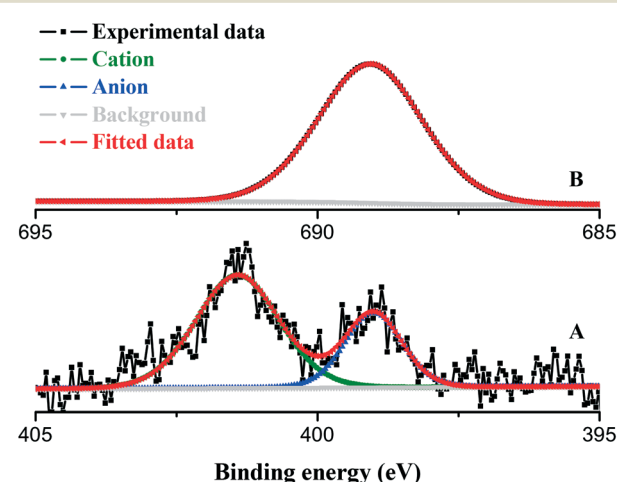


Fig. 5 XP spectra of CARB80 A) N 1s and B) F 1s.



Table 3 SILP hydrogenation<sup>a</sup> of aldehydes A1–A4 with catalyst 1 immobilized on carbon (CARB80) and silica (SILP20) supports

$\text{R}-\text{CHO} \xrightarrow[5 \text{ mol\% DBU}]{\text{H}_2, n\text{-heptane}, 25^\circ\text{C}} \text{R}-\text{CH}_2\text{OH}$

A1
A2
A3
A4

Entry	Aldehyde	Support	S/C	P (bar)	Time (min)	Conversion <sup>c</sup> (%)	TON	TOF (h <sup>-1</sup> )
1	A1	CARB80	200	10	90	8	16	11
2	A1	CARB80	200	20	90	45	90	60
3	A1	CARB80	200	30	90	52	104	69
4	A1	CARB80	200	40	90	60	120	80
5	A1	CARB80	1000	40	90	16	160	107
6	A1	CARB80	200	10	180	>99	200	67
7 <sup>b</sup>	A1	SILP20	200	10	17	>99	200	706
8	A2	CARB80	200	10	240	>99	200	50
9 <sup>b</sup>	A2	SILP20	200	10	60	>99	200	200
10	A3	CARB80	200	10	240	>99	200	50
11 <sup>b</sup>	A3	SILP20	200	10	60	>99	200	200
12	A4	CARB80	200	10	240	>99	200	50
13 <sup>b</sup>	A4	SILP20	200	10	60	>99	200	200

<sup>a</sup> Conditions: entry 1–4, 6, 8, 10, 12: 2 mmol substrate, 180 mg of CARB80 (5 mg of 1, 75 mg of IL, 100 mg of CARB); entry 5: 10 mmol substrate, 180 mg of CARB80 (5 mg of 1, 75 mg of IL, 100 mg of CARB). <sup>b</sup> Previous results.<sup>21</sup> <sup>c</sup> Determined by <sup>19</sup>F{<sup>1</sup>H} or <sup>1</sup>H NMR spectroscopy.

reported recently also with silica-based SILP catalysts.<sup>21</sup> In all cases, quantitative conversion was obtained, yet, at significantly slower reaction rates with the catalyst immobilized in the carbon matrix CARB80. The main reason for this different performance of carbon- and silica-based SILP catalysts is believed to lie in the different pore

sizes of these two support materials. The silica used in the SILP20 catalyst is a typical mesoporous material with pore diameters in the 5–15 nm range. With an estimated thickness of ~0.6 nm for a monolayer of [C<sub>2</sub>m<sub>2</sub>im][NTf<sub>2</sub>],<sup>22</sup> these pores can be coated with several layers of IL/catalyst solution and still remain open pores with high surface area

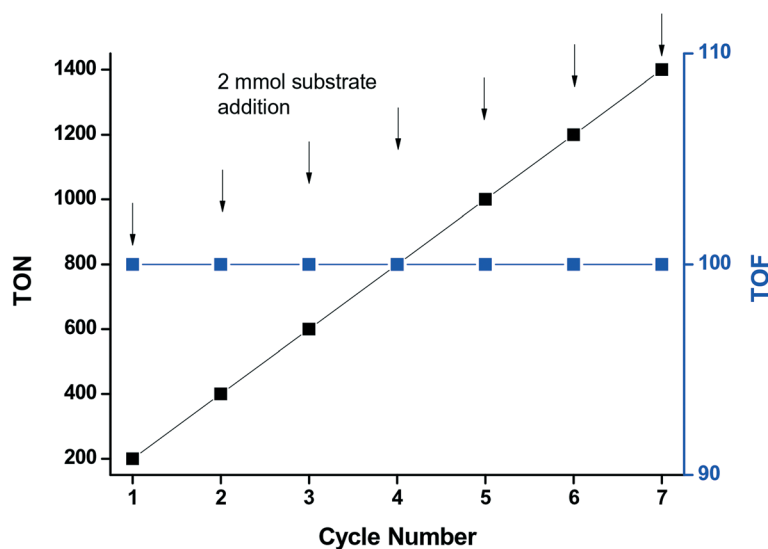


Fig. 6 Catalyst recycling in the hydrogenation of 4-fluorobenzaldehyde by repeated addition of aldehyde (conditions: CARB80, 2 mL *n*-heptane, 2 mmol substrate, 5 mol% DBU, 25 °C, 40 bar H<sub>2</sub>).



and easy access for the reaction solution. The carbon support used in this work, on the other hand, contains a high percentage of micropores with diameters  $<2$  nm, which are either inaccessible ( $d < 0.6$  nm) or completely filled with  $[\text{C}_2\text{m}_2\text{im}][\text{NTf}_2]$ , as evidenced by the steep rise of the  $\text{N}_2$  adsorption isotherm at low pressures (Fig. 3A). The slower conversion compared to the silica support might therefore be caused primarily by the smaller interface area and the larger diffusion paths of the carbon-based SILP catalysts.

The sustainability of CARB80 was tested by repeated addition of aldehyde immediately after the end of the reaction (Fig. 6). This procedure was carried out six times every 2 hours and yielded an overall TON of 1400 at a constant rate of conversion ( $\text{TOF} = 100 \text{ h}^{-1}$ ). These results hold great promise for a continuous flow operation of this catalytic system without a significant loss of activity in prolonged operation. Iron leaching, measured after all the reactions by ICP-OES, was below 0.3 mol% with respect to the initial loading, while IL leaching was not detected at all by  $^{19}\text{F}\{^1\text{H}\}$  NMR spectroscopy. On the contrary, we observed extensive IL leaching in preliminary experiments with mesoporous carbon with average pore diameters in the 5–10 nm range, in support of our presumption that the smaller pore sizes of our current, microporous support prevent IL leaching. Untreated carbon is known to have a rather hydrophobic surface (water contact angle  $\sim 90^\circ$ )<sup>23</sup> and is also only partly wetted by ionic liquids (contact angle of  $[\text{C}_2\text{C}_1\text{im}][\text{NTf}_2]$  on graphite =  $44^\circ$ )<sup>24</sup>. Increasing the affinity between the ionic liquid and the carbon surface by coating it with an “IL-philic” layer should strengthen the confinement of the ionic liquid in the pores and repress IL leaching also for mesoporous carbon substrates. This is currently being investigated in our group.

## Conclusions

In the present work, a carbon-based SILP catalytic system was tested for the hydrogenation of aldehydes, comprising micro/mesoporous activated carbon spheres impregnated with an  $\text{Fe}(\text{n})$  PNP pincer complex catalyst dissolved in an imidazolium-based IL. We characterized the carbon support, which was used as received without any surface modification, and the SILP *via* FTIR, BET, and XPS measurements. The influence of the hydrogen pressure and the substrate/catalyst ratio on the reaction yield and the TON and TOF values was investigated and compared to previous results obtained with a silica-based SILP system. The best carbon SILP system was catalytically active under mild conditions, without significant leaching of IL or catalyst and gave quantitative conversions for all investigated aldehydes, yet at substantially longer reaction times compared to the previous silica SILP system.<sup>21</sup> Catalyst recycling experiments through repeated substrate addition showed unaltered quantitative conversion over four reaction cycles and showed great promise for a continuous flow operation of this catalytic system.

## Conflicts of interest

There are no conflicts to declare.

## Acknowledgements

ZC, JB, and KK thank the Austrian Science Fund (FWF) for the financial support through projects M 2068-N28 (ZC) and P28866-N34 (JB, KK). NY and GR acknowledge financial support by FWF *via* the Doctorate School Solids4Fun (DK+ W1243).

## References

- (a) *Handbook of Homogeneous Hydrogenation*, ed. J. G. de Vries and C. J. Elsevier, Wiley-VCH, Weinheim, 2007; (b) P. Dupau, in *Organometallics as Catalysts in the Fine Chemical Industry*, ed. M. Beller and H. U. Blaser, Springer-Verlag, Berlin, 2012; (c) N. B. Johnson, I. C. Lennon, P. H. Moran and J. A. Ramsden, *Acc. Chem. Res.*, 2007, **40**, 1291–1299; (d) P. A. Dub and T. Ikariya, *ACS Catal.*, 2012, **2**, 1718–1741.
- (a) H. U. Blaser, C. Malan, B. Pugin, F. Spindler, H. Steiner and M. Studer, *Adv. Synth. Catal.*, 2003, **345**, 103–151; (b) F. Naud, F. Spindler, C. J. Rueggeberg, A. T. Schmidt and H. U. Blaser, *Org. Process Res. Dev.*, 2007, **11**, 519–523; (c) R. Noyori and T. Ohkuma, *Angew. Chem., Int. Ed.*, 2001, **40**, 40–73; (d) R. Noyori, *Angew. Chem., Int. Ed.*, 2013, **52**, 79–92.
- Mn-catalyzed hydrogenation reactions: (a) N. A. Espinosa-Jalapa, A. Nerush, L. J. W. Shimon, G. Leitus, L. Avram, Y. Ben-David and D. Milstein, *Chem. – Eur. J.*, 2017, **23**, 5934–5938; (b) F. Kallmeier, T. Irrgang, T. Dietel and R. Kempe, *Angew. Chem., Int. Ed.*, 2016, **55**, 11806–11809; (c) S. Elangovan, C. Topf, S. Fischer, H. Jiao, A. Spannenberg, W. Baumann, R. Ludwig, K. Junge and M. Beller, *J. Am. Chem. Soc.*, 2016, **138**, 8809–8814; (d) S. Elangovan, M. Garbe, H. Jiao, A. Spannenberg, K. Junge and M. Beller, *Angew. Chem., Int. Ed.*, 2016, **55**, 15364–15368; (e) V. Papa, J. R. Cabrero-Antonio, E. Alberico, A. Spannenberg, K. Junge, H. Junge and M. Beller, *Chem. Sci.*, 2017, **8**, 3576–3585; (f) A. Bruneau-Voisine, D. Wang, T. Roisnel, C. Darcel and J.-P. Sortais, *Catal. Commun.*, 2017, **92**, 1–4; (g) M. B. Widegren, G. J. Harkness, A. M. Z. Slawin, D. B. Cordes and M. L. Clarke, *Angew. Chem., Int. Ed.*, 2017, **56**, 5825–5828; (h) F. Bertini, M. Glatz, N. Gorgas, B. Stöger, M. Peruzzini, L. F. Veiros, K. Kirchner and L. Gonsalvi, *Chem. Sci.*, 2017, **8**, 5024–5029; (i) M. Glatz, B. Stöger, D. Himmelbauer, L. F. Veiros and K. Kirchner, *ACS Catal.*, 2018, **8**, 4009–4016; (j) N. Gorgas and K. Kirchner, *Acc. Chem. Res.*, 2018, **51**, 1558–1569.
- Fe-catalyzed hydrogenation reactions: (a) C. Federsel, A. Boddien, R. Jackstell, R. Jennerjahn, P. J. Dyson, R. Scopelliti, G. Laurenczy and M. Beller, *Angew. Chem., Int. Ed.*, 2010, **49**, 9777–9780; (b) R. Langer, G. Leitus, Y. Ben-David and D. Milstein, *Angew. Chem., Int. Ed.*, 2011, **50**, 2120–2124; (c) R. Langer, M. A. Iron, L. Konstantinovski, Y. Diskin-Posner, G. Leitus, Y. Ben-David and D. Milstein, *Chem. – Eur. J.*, 2012, **18**, 7196–7209; (d) C. Ziebart, C. Federsel, P. Anbarasan, R. Jackstell, W. Baumann, A.





Spannenberg and M. Beller, *J. Am. Chem. Soc.*, 2012, **134**, 20701–20704; (e) S. Fleischer, S. Zhou, K. Junge and M. Beller, *Angew. Chem., Int. Ed.*, 2013, **52**, 5120–5124; (f) D. Srimani, Y. Diskin-Posner, Y. Ben-David and D. Milstein, *Angew. Chem., Int. Ed.*, 2013, **52**, 14131–14134; (g) G. Wienhofer, M. Baseda-Kruger, C. Ziebart, F. A. Westerhaus, W. Baumann, R. Jackstell, K. Junge and M. Beller, *Chem. Commun.*, 2013, **49**, 9089–9091; (h) C. Bornschein, S. Werkmeister, B. Wendt, H. Jiao, E. Alberico, W. Baumann, H. Junge, K. Junge and M. Beller, *Nat. Commun.*, 2014, **5**, 4111; (i) S. Chakraborty, H. Dai, P. Bhattacharya, N. T. Fairweather, M. S. Gibson, J. A. Krause and H. Guan, *J. Am. Chem. Soc.*, 2014, **136**, 7869–7872; (j) S. Chakraborty, P. O. Lagaditis, M. Förster, E. A. Bielinski, N. Hazari, M. C. Holthausen, W. D. Jones and S. Schneider, *ACS Catal.*, 2014, **4**, 3994–4003; (k) P. O. Lagaditis, P. E. Sues, J. F. Sonnenberg, K. Y. Wan, A. J. Lough and R. H. Morris, *J. Am. Chem. Soc.*, 2014, **136**, 1367–1380; (l) S. Werkmeister, K. Junge, B. Wendt, E. Alberico, H. Jiao, W. Baumann, H. Junge, F. Gallou and M. Beller, *Angew. Chem., Int. Ed.*, 2014, **53**, 8722–8726; (m) F. Bertini, I. Mellone, A. Ienco, M. Peruzzini and L. Gonsalvi, *ACS Catal.*, 2015, **5**, 1254–1265; (n) O. Rivada-Wheelaghan, A. Dauth, G. Leitus, Y. Diskin-Posner and D. Milstein, *Inorg. Chem.*, 2015, **54**, 4526–4538; (o) Y. Zhang, A. D. MacIntosh, J. L. Wong, E. A. Bielinski, P. G. Williard, B. Q. Mercado, N. Hazari and W. H. Bernskoetter, *Chem. Sci.*, 2015, **6**, 4291–4299; (p) N. Gorgas, B. Stöger, L. F. Veiros, E. Pittenauer, G. Allmaier and K. Kirchner, *Organometallics*, 2014, **33**, 6905–6914; (q) G. Wienhofer, F. A. Westerhaus, K. Junge, R. Ludwig and M. Beller, *Chem. – Eur. J.*, 2013, **19**, 7701–7707; (r) T. Zell, Y. Ben-David and D. Milstein, *Catal. Sci. Technol.*, 2015, **5**, 822–826; (s) S. Mazza, R. Scopelliti and X. Hu, *Organometallics*, 2015, **34**, 1538–1545.

5 N. Gorgas, B. Stöger, L. F. Veiros and K. Kirchner, *ACS Catal.*, 2016, **6**, 2664–2672.

6 (a) M. Heitbaum, F. Glorius and I. Escher, *Angew. Chem., Int. Ed.*, 2006, **45**, 4732–4762; (b) P. McMorn and G. J. Hutching, *Chem. Soc. Rev.*, 2004, **33**, 108–122; (c) D. J. Xuereb, J. Dzierzak and R. Raja, *Catal. Today*, 2012, **198**, 19–34; (d) A. Corma and H. Garcia, *Adv. Synth. Catal.*, 2006, **348**, 1391–1412; (e) A. J. Sandee, J. N. H. Reek, P. C. J. Kamer and P. W. N. M. van Leeuwen, *J. Am. Chem. Soc.*, 2001, **123**, 8468–8476; (f) J. Govan and Y. K. Gun'ko, *Nanomaterials*, 2014, **4**, 222–241; (g) S. Sabater, J. A. Mata and E. Peris, *ACS Catal.*, 2014, **4**, 2038–2047; (h) G. Varga, Z. Timár, S. Muráth, Z. Kónya, Á. Kukovecz, S. Carlson, P. Sipos and I. Pálunkó, *Top. Catal.*, 2017, **60**, 1429–1438; (i) S. A. Burgess, A. Kassie, S. A. Baranowski, K. J. Fritzsching, K. Schmidt-Rohr, C. M. Brown and C. R. Wade, *J. Am. Chem. Soc.*, 2016, **138**, 1780–1783.

7 (a) H.-P. Steinrück and P. Wasserscheid, *Catal. Lett.*, 2015, **145**, 380–397; (b) A. Riisager, K. Michael Eriksen, P. Wasserscheid and R. Fehrmann, *Catal. Lett.*, 2003, **90**, 149–153; (c) T. Selvam, A. Machoke and W. Schwieger, *Appl. Catal., A*, 2012, **445–446**, 92–101; (d) R. Sheldon, *Chem. Commun.*, 2001, 2399–2407; (e) C. Van Doorslaer, J. Wahlen, P. Mertens, K. Binnemans and D. De Vos, *Dalton Trans.*, 2010, **39**, 8377–8390; (f) Q. Zhang, S. Zhang and Y. Deng, *Green Chem.*, 2011, **13**, 2619–2637; (g) T. J. Geldbach and P. J. Dyson, *J. Am. Chem. Soc.*, 2004, **126**, 8114–8115; (h) C. P. Mehnert, *Chem. – Eur. J.*, 2005, **11**, 50–56; (i) A. Riisager, R. Fehrmann, M. Haumann and P. Wasserscheid, *Eur. J. Inorg. Chem.*, 2006, 695–706; (j) P. Wasserscheid and W. Keim, *Angew. Chem., Int. Ed.*, 2000, **39**, 3772–3789; (k) Z. Zhang, G. Franciò and W. Leitner, *ChemCatChem*, 2015, **7**, 1961–1965; (l) F. Giacalone and M. Gruttaduria, *ChemCatChem*, 2016, **8**, 664–684; (m) R. Fehrmann, A. Riisager and M. Haumann, *Supported Ionic Liquids: Fundamentals and Applications*, Wiley-VCH, Weinheim, 2014.

8 (a) A. Schönweiz, S. Werner, R. Franke, K.-D. Wiese, M. Haumann and P. Wasserscheid, *Angew. Chem., Int. Ed.*, 2011, **50**, 4492–4495; (b) U. Hintermair, G. Zhao, C. C. Santini, M. J. Muldoon and D. J. Cole-Hamilton, *Chem. Commun.*, 2007, 1462–1464; (c) A. Riisager, B. Jorgensen, P. Wasserscheid and R. Fehrmann, *Chem. Commun.*, 2006, 994–996; (d) M. Ruta, I. Yuranov, P. J. Dyson, G. Laurencey and L. Kiwi-Minsker, *J. Catal.*, 2007, **247**, 269–276; (e) U. Hintermair, T. Höfener, T. Pullmann, G. Francio and W. Leitner, *ChemCatChem*, 2010, **2**, 150–154; (f) U. Hintermair, G. Francio and W. Leitner, *Chem. – Eur. J.*, 2013, **19**, 4538–4547; (g) J. Scholz, S. Loekman, N. Szesni, W. Hieringer, A. Görling, M. Haumann and P. Wasserscheid, *Adv. Synth. Catal.*, 2011, **353**, 2701–2707; (h) J. Joni, M. Haumann and P. Wasserscheid, *Appl. Catal., A*, 2010, **372**, 8–15; (i) S. Werner, N. Szesni, R. W. Fischer, M. Haumann and P. Wasserscheid, *Phys. Chem. Chem. Phys.*, 2009, **11**, 10817–10819; (j) S. Werner, N. Szesni, M. Kaiser, R. W. Fischer, M. Haumann and P. Wasserscheid, *ChemCatChem*, 2010, **2**, 1399–1402.

9 (a) J. Palomar, J. Lemus, M. A. Gilarranz and J. J. Rodriguez, *Carbon*, 2009, **47**, 1846–1856; (b) P. Virtanen, H. Karhu, K. Kordas and J.-P. Mikkola, *Chem. Eng. Sci.*, 2007, **62**, 3660–3671; (c) M. Rufete-Beneite, M. C. Roman-Martinez and A. Linares-Solano, *Carbon*, 2014, **77**, 947–957; (d) J. Lemus, J. Palomar, M. A. Gilarranz and J. J. Rodriguez, *Adsorption*, 2011, **17**, 561–571; (e) H. Klefer, M. Munoz, A. Modrow, B. Böhringer, P. Wasserscheid and B. J. M. Etzold, *Chem. Eng. Technol.*, 2016, **39**, 276–284; (f) A. Weiß, M. Munoz, A. Haas, F. Rietzler, H.-P. Steinrück, M. Haumann, P. Wasserscheid and B. J. M. Etzold, *ACS Catal.*, 2016, **6**, 2280–2286.

10 M. Rufete-Beneite and M. C. Roman-Martinez, *RSC Adv.*, 2016, **6**, 100976–100983.

11 A. Weiß, M. Giese, M. Lijewski, R. Franke, P. Wasserscheid and M. Haumann, *Catal. Sci. Technol.*, 2017, **7**, 5562–5571.

12 D. D. Perrin and W. L. F. Armarego, *Purification of Laboratory Chemicals*, Pergamon, New York, 1988, 3rd edn.

13 (a) D. A. Shirley, *Phys. Rev. B: Solid State*, 1972, **5**, 4709–4714; (b) S. Tougaard, *Surf. Interface Anal.*, 1997, **25**, 137–154.

14 J. H. Scofield, *J. Electron Spectrosc. Relat. Phenom.*, 1976, **8**, 129–137.

15 C. Peng, J. Lang, S. Xu and X. Wang, *RSC Adv.*, 2014, **4**, 54662–54667.

16 M. S. Shafeeyan, W. M. A. W. Daud, A. Houshmand and A. Shamiri, *J. Anal. Appl. Pyrolysis*, 2010, **89**, 143–151.

17 H. Guedidi, L. Reinert, J.-M. Leveque, Y. Soneda, N. Bellakhal and L. Duclaux, *Carbon*, 2013, **54**, 432–443.

18 P. Schneider, *Appl. Catal., A*, 1995, **129**, 157–259.

19 M. Sobota, I. Nikiforidis, W. Hieringer, N. Paape, M. Happel, H.-P. Steinrück, A. Görling, P. Wasserscheid, M. Laurin and J. Libuda, *Langmuir*, 2010, **26**, 7199–7207.

20 K. Dong, L. Zhao, Q. Wang, Y. Song and S. Zhang, *Phys. Chem. Chem. Phys.*, 2013, **15**, 6034–6040.

21 J. Brünig, Z. Csendes, S. Weber, N. Gorgas, R. W. Bittner, A. Limbeck, K. Bica, H. Hoffmann and K. Kirchner, *ACS Catal.*, 2018, **8**, 1048–1051.

22 S. Bovio, A. Podesta, C. Lenardi and P. Milani, *J. Phys. Chem. B*, 2009, **113**, 6600–6603.

23 Z. Li, Y. Wang, A. Kozbial, G. Shenoy, F. Zhou, R. McGinley, P. Ireland, B. Morganstein, A. Kunkel, S. P. Surwade, L. Li and H. Liu, *Nat. Mater.*, 2013, **12**, 925–931.

24 E. Bordes, L. Douce, E. L. Quivetis, A. A. H. Padua and M. C. Gomes, *J. Chem. Phys.*, 2018, **148**, 193840.

